Materials Today Bio 26 (2024) 101097

Contents lists available at ScienceDirect

Materials Today Bio

journal homepage: www.journals.elsevier.com/materials-today-bio

Cellular memory function from 3D to 2D: Three-dimensional high density collagen microfiber cultures induce their resistance to reactive oxygen species

Asuka Yamada [a,b,c], Shiro Kitano [a,b,**], Michiya Matsusaki [b,c,*]

[a] TOPPAN HOLDINGS INC. Business Development Division, Technical Research Institute, Takanodaiminami, Sugito-machi, Saitama 345-8508, Japan
[b] Joint Research Laboratory (TOPPAN) for Advanced Cell Regulatory Chemistry, Graduate School of Engineering, Osaka University, Yamadaoka, Suita, Osaka 565-0871, Japan
[c] Division of Applied Chemistry, Graduate School of Engineering, Osaka University, Yamadaoka, Suita, Osaka 565-0871, Japan

ARTICLE INFO

Keywords:
3D culture
Collagen microfibers
Cancer tissue
Reactive oxygen species
Cellular memory function

ABSTRACT

Cell properties generally change when the culture condition is changed. However, mesenchymal stem cells cultured on a hard material surface maintain their differentiation characteristics even after being cultured on a soft material surface. This phenomenon suggests the possibility of a cell culture material to memorize stem cell function even in changing cell culture conditions. However, there are no reports about cell memory function in three-dimensional (3D) culture. In this study, colon cancer cells were cultured with collagen microfibers (CMF) in 3D to evaluate their resistance to reactive oxygen species (ROS) in comparison with a monolayer (2D) culture condition and to understand the effect of 3D-culture on cell memory function. The ratio of ROS-negative cancer cells in 3D culture increased with increasing amounts of CMF and the highest amount of CMF was revealed to be 35-fold higher than that of the 2D condition. The ROS-negative cells ratio was maintained for 7 days after re-seeding in a 2D culture condition, suggesting a 3D-memory function of ROS resistance. The findings of this study will open up new opportunities for 3D culture to induce cell memory function.

1. Introduction

Cell properties typically change as the form of culture changes. In particular, stem cells are said to respond to mechanical signals presented by the extracellular matrix (ECM). Studies in this area have been based on the principle of cellular mechanotransduction, the hypothesis that cells sense and integrate mechanical cues from the ECM, ultimately directing gene expression and cell fate decisions. Anseth and co-worker have suggested that mechanical stimuli, related to tissue stiffness, are retained as a historical influence and affect differentiation, particularly in mesenchymal stem cells [1]. As a mechanism, they concluded that it is associated with a state in which the known inactivation target molecules of the Hippo signaling pathway, such as Yes-associated protein (YAP) and Runt-related transcription factor 2 (RUNX2), remain migrated and maintained in the nucleus. Elsewhere, it has been reported that in skeletal muscle cells, hydrogel stiffness activates myocytes and induces proliferation and migration [2]. It has also been reported that fibroblasts cultured on stiff hydrogels maintain their cytoskeleton on stiff gels even after the gels soften [3]. This is an important and interesting study because of the various possible applications regarding the effect of culture history on the long-term properties of cells, but no similar studies by other groups have been reported. In addition, in the above study, synthetic polymers such as polyethylene glycol (PEG) were used as models for the scaffold material hydrogel. Synthetic polymers do not have cell adhesion domains, so it is not possible to evaluate the influence of adhesion signaling by the ECM. For example, in cancer, the stiffness of the stromal tissue consisting of the ECM is said to affect prognosis. In fact, clinical studies of colorectal cancer have reported that patients with

Abbreviations: 2D, two-dimensional; 3D, three-dimensional; DMEM, Dulbecco's modified Eagle medium; ECM, extracellular matrix; CMF, Collagen microfibers; ROS, Reactive oxygen species; FBS, fetal bovine serum; PBS, phosphate-buffered saline; ANS-8, Magnesium [II] 8-Anilino-1-naphthalenesulfonate; TBHP, *tert*-Butyl hydroperoxide; GCL, Glutamate-cysteine ligase; GSR, Glutathione reductase; HIF1α, Hypoxia inducing factor 1a; BNIP3, Bcl-2 interacting protein 3; PDK1, Pyruvate dehydrogenase kinase 1; YAP, Yes-associated protein; TAZ (WWTR), WW Domain Containing Transcription Regulator; PPIA, Peptidylprolyl isomerase A.

* Corresponding author. Department of Applied Chemistry Graduate School of Engineering Osaka University 2-1 Yamadaoka, Suita, Osaka 565-0871, Japan.
** Corresponding author. TOPPAN HOLDINGS INC. TOPPAN Technical Research Institute, Takanodaiminami, Sugito-machi, Saitama 345-8508, Japan.
E-mail addresses: shiro.kitano@toppan.co.jp (S. Kitano), m-matsusaki@chem.eng.osaka-u.ac.jp (M. Matsusaki).

https://doi.org/10.1016/j.mtbio.2024.101097
Received 10 February 2024; Received in revised form 14 May 2024; Accepted 21 May 2024
Available online 22 May 2024

high tumor elasticity tend to have lower survival rates and more advanced tumor stages compared to patients with low elasticity [4]. There are reports that the combination of drugs that soften stromal tissue and molecularly-targeted drugs actually improved the survival rate of patients with colorectal cancer [5]. Thus, colon cancer cells are thought to be affected by the surrounding environment, but the historical effects of the surrounding environment have not been reported. It is important to study *in vitro* cancer models that can control both ECM and stiffness in both drug and pathological evaluation models over an extended period. Cell memory function in 3D culture is another key area for future study.

One of the difficulties in developing *in vitro* cancer models for evaluating anticancer drugs is the reproduction of drug resistance. Malignant cancer cells, including cancer stem cells, are resistant to chemotherapy, causing postoperative recurrence and metastasis [6]. It is reported that this is due to the resistance to long-term stress. Malignant cancer cells are said to be constantly exposed to oxidative stress due to the generation of reactive oxygen species (ROS) by anticancer drugs and metabolites [7]. Cancer cells can survive for long periods of time because they are resistant to such stress. Hence, even though cancer stem cells are present in only small numbers, they have the ability to form tumors similar to the original major tissues. Most cultured cancer cells, including cell lines, have lost this stem cell nature [8], and the results of drug efficacy evaluation are often more responsive than *in vivo* results [9].

One reason for this is that *in vitro* models do not replicate the human body's environment, including collagen and other ECM components, and the oxygen levels are in a unique hypoxic state known as intratumoral hypoxia [10]. Spheroids, a conventional 3D technology, have the advantage of promoting intercellular adhesion by stacking cells in a spherical shape. It has been reported that spheroids co-cultured with stromal cells other than cancer cells show a difference in efficacy compared to spheroids composed of single cells, especially in pancreatic cancer, which is greatly affected by stromal tissue [11]. However, spheroids have a very high density of cells, and above a certain size the central part is prone to necrosis because it is difficult to supply nutrients to the interior [12]. For this reason, porous scaffolds with oxygen permeability have also been considered in scaffold-based 3D technology. Because of their ability to supply nutrients internally and to withstand long-term incubation, their development for numerous transplantation applications have been reported [13]. However, for application to *in vitro* models, it is difficult to disperse cells within the scaffold. While numerous methods have been reported for embedding cells uniformly in hydrogels [14], it is challenging to reproduce ECM, particularly interstitial tissues with significant collagen content, using hydrogels made solely of synthetic polymers like PEG.

To construct more complex tissues, some authors have reported the introduction of vascular networks and lymphatic vessels within the 3D model by coating ECM and multiple cells. In this system, researchers succeeded in reproducing the lumenal structure in cancer stromal tissue and liver tissues [15,16]. In terms of scaffolding materials, collagen is the most widely used ECM because of its high cell adhesion and gelation properties. However, collagen has low solubility in water [17], making it difficult to prepare collagen solutions with concentrations above a certain level. *In vitro* 3D models with higher density ECM are needed to reproduce the interstitial tissues of living organisms [18].

Previously, it was discovered that collagen microfibers (CMF) with micrometer-level fiber length can be created by homogenizing

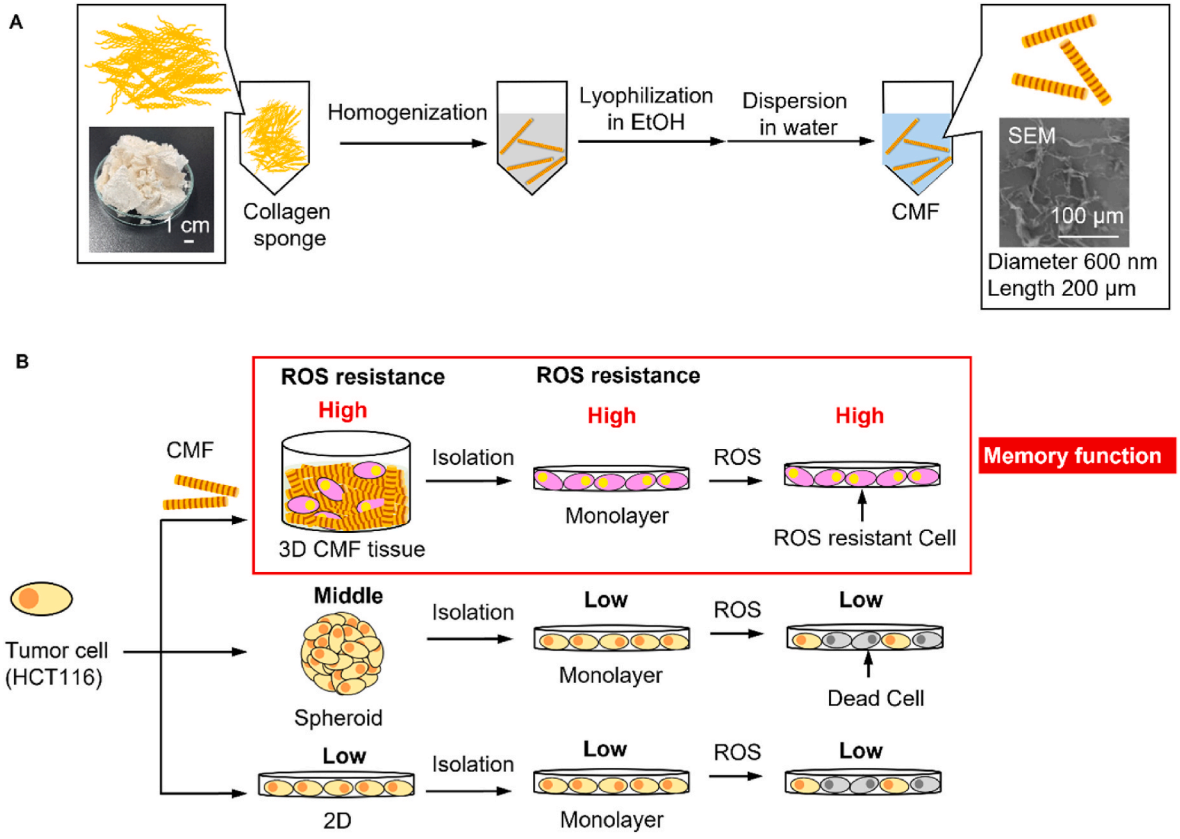

Fig. 1. (A) Fabrication process of CMF, collagen sponge was homogenized at 0.1 mg mL^{-1} in 85 % ethanol for 6 min and in 70 % ethanol for 1 min subsequently at 4 °C. The obtained CMF was washed with ultra-pure water and lyophilized for 4 days. (B) Schematic illustration of "memory function" of tumor cells isolated from CMF 3D composed of CMF and colorectal cancer cells (HCT116). HCT116 were pre-cultured for 7 days in three different conditions, CMF 3D, spheroid and 2D respectively. The isolated cancer cells were cultured in a monolayer condition for 11 days and the consumed amount of ROS added in culture medium was measured during the culture period to evaluate ROS resistance.

lyophilized collagen in an aqueous solution (Fig. 1A). This CMF does not dissolve in the culture medium and can be mixed with cells in suspension to create 3D tissues with as much as 20–30 % dense collagen [19,20]. This proprietary material was applied to gingival models with collagen-dense dermal layers and to adipose tissue models with mature fat and vascular networks, which are difficult to achieve with conventional 3D culture [21,22]. In non-human animal species, CMF has been used as an ink for 3D bioprinters due to its low viscosity relative to concentration when forming cultured meat using three cell types isolated from cattle [23]. However, there have been no reports of the use of CMF in cancer models, where the contribution of collagen cells is considered important. In addition, the effects of conventional 3D techniques on cancer cell properties, such as drug resistance and stemness, have been observed to be different from those of 2D culture.

Herein, we report that colon cancer cells (HCT116) were cultured with CMF in 3D to evaluate their resistance to ROS in comparison with a monolayer (2D) culture condition and to understand the effect of 3D-culture on cell memory function. The ratio of ROS-negative cancer cells in 3D culture increased with increasing amounts of CMF and the highest amount of CMF was revealed to be 35-fold higher than that of the 2D condition. It was suggested that this property is maintained at the genetic level even after the scaffold material is removed and the cells are returned to 2D culture (Fig. 1B).

2. Experimental section

2.1. Fabrication of CMF

17 mL of 3 mg mL^{-1} collagen solution (PSC-1-200-100, NIPPI, Tokyo, Japan) was gelated with neutralization buffer containing 0.05 N sodium hydroxide (Nacalai Tesque, INC., Kyoto, Japan) and 10 × phosphate-buffered saline (PBS) (07269-84, Nacalai Tesque. INC.) mixed at a ratio of 1:1 for 1 h at 37 °C. Collagen gel was frozen by liquid N_2 and lyophilized for 72 h with a freeze dryer (FDU-2200, EYELA, Tokyo, Japan). Dried collagen gel was homogenized with a homogenizer (T 10 basic ULTRA-TURRAX, IKA® Japan K·K., Osaka, Japan) in 85 % ethanol. The collagen suspension was centrifuged for 3 min at 9000×*g*. After removal of the supernatant, collagen pellets were homogenized in 70 % ethanol. Collagen suspension is centrifuged for a further 3 min at 9000×*g*. After removal of the supernatant, collagen pellets were washed by distilled water 2 times. The collagen suspension was sonicated by an ultrasonicater 10 times for 20 min with 50 W at 20 kHz (VC-50, Sonics & Materials, Inc., Newtown, CT, USA) and lyophilized for 72 h.

2.2. Scanning electron microscope (SEM) imaging

Dried collagen sponge and CMF were coated with osmium for conductivity and observed using a Field Emission SEM (Merlin, Carl Zeiss AG, Oberkochen, Germany) with an acceleration voltage of 0.8 kV.

2.3. Circular Dichroism (CD) spectrum

CMF and native collagen were dissolved in 5 mM acetic acid to 5 μg mL^{-1}. Circular Dichroism (CD) measurements were taken using a spectropolarimeter (J–1100, JASCO, Tokyo, Japan). The optical path length was 10 mm and the scanning speed was 100 nm min^{-1}. All the CD measurements were taken at 25 °C.

2.4. Hydrophobicity assay

CMF and native collagen were dissolved in PBS to 5 mg mL^{-1}. Magnesium [II] 8-Anilino-1-naphthalenesulfonate (ANS-8 Mg) (A5353, TCI, Tokyo, Japan) was dissolved in 1 × PBS to 250 μM 200 μL of ANS-Mg/PBS solution were added to 500 μL of collagen sample and incubated for 1 h at 25 °C. The excitation wavelength for ANS fluorescence was set at 380 nm and the emission spectra were recorded from 400 to 600 nm by spectrophotometer (Nanodrop-3300, Thermo Fisher Scientific, Eugene, MA, USA).

2.5. Cell culture

HCT116, MDA-MB-231 and HT29 cells were obtained from USA Type Cell Collection (Manassas, VA, USA). Normal human dermal fibroblast (NHDF) cells were obtained from Lonza Japan (Tokyo, Japan). HCT116, MDA-MB-231 and NHDF cells were maintained in Dulbecco's modified Eagle medium (DMEM) (08458-16, Nacalai Tesque, INC.) supplemented with 10 % fetal bovine serum (FBS) (Thermo Fisher Scientific), 100 U mL^{-1} penicillin, 100 μg mL^{-1} streptomycin and 0.25 μg mL^{-1} amphotericin B (02892-54, Nacalai Tesque. INC.). HT29 was maintained in McCoy's 5A (Modified) Medium (Thermo Fisher Scientific) with 10 % FBS. After 7 days culture in 5 % CO_2 at 37 °C, cells were trypsinized and suspended in the culture medium.

2.6. Development of CMF 3D tissue

60 mg of dried CMF was mixed with 6 mL of distilled water by vigorous shaking. The CMF suspension was centrifuged for 1 min at 9000×*g*. After removal of the supernatant, 3600 μL of distilled water was added into the tube and then mixed by pipetting. 1, 5 and 10 mg of CMF suspension were dispensed into 1.5 mL tubes. 1.0×10^6 of cells in the medium was mixed with each CMF suspension by pipetting. The mixture of CMF and cells was centrifuged for 1 min at 9000×*g*. After removal of the supernatant, each sediment was dispersed into the medium by pipetting and seeded on a Transwell® (#3470, Corning, Corning, NY, USA).

2.7. Compression test

CMF tissues were fabricated as described in 2.5. using 1, 5 and 10 mg of CMF and 1.0×10^6 HCT116 cells and then incubated at 37 °C for 7 days in 24 well insert. Obtained CMF tissues were cylindrical and 6.5 mm in diameter. Sample height of 1,5 and 10 mg of CMF tissue was 0.5 mm 2 mm and 3 mm, respectively. The elastic moduli of the CMF tissues were measured using a compression tester (EZ-Test, SHIMADZU, Kyoto, Japan). Compression test was performed the speed at 1 mm sec^{-1} with at room temperature using 5 mm spherical probe and 20 N load cell. The elastic modulus E (kPa) was calculated using the following equation, where S is the slope of the stress-strain curve (mN mm^{-1}), H is the height of the gel (mm) and C is the contact area of the testing jig with the gel (mm^2)

$$E = S \times H/C$$

The slope of the graph was selected to follow the rising edge of the stress-strain curve at strains between 5 and 10 %, the height of the gel was measured using a digital caliper (Digimatic Caliper CD-15CP, Mitsutoyo, Kanagawa, Japan), and the contact area of the jig was calculated by integrating the strain values in the stress-strain curve.

2.8. 2D culture and spheroid culture

Monolayer 2D cultures were performed using a 6-well plate (1810-006 N, AGC TECHNO GLASS, Shizuoka, Japan). Spheroid cultures were performed using a PrimeSurface® 96 slit-well plate (MS-9096S, Sumitomo Bakelite, Tokyo, Japan). HCT116 cells were seeded at 1.0×10^4 per well for 2D and 5.0×10^3 per well for spheroids. All cells were cultured at 37 °C in 5 % CO_2.

2.9. ROS analysis

After 7 days culture for each method, cells were isolated with Accumax (17087-54, Nacalai Tesque, INC.) and 2 mg mL^{-1} collagenase (9001-12-1, FUJIFILM Wako Pure Chemical Corporation, Osaka, Japan)

from scaffolds. Cells were passed through 100 μm and 40 μm filters sequentially. 100 μM of *tert*-Butyl hydroperoxide (TBHP) was added to each sample as the source of ROS. After 30 min incubation in 37 °C, TBHP was removed by centrifugation and intracellular ROS levels of 5.0×10^5 of cells for each culture method were assayed by CellROX™ Deep Red Flow Cytometry Assay Kit (C10491, Thermo Fisher Scientific) using FACS Melody (Becton Dickinson, New Jersey, USA). ROS-negative cells were defined as the population of ROS-negative cells in the subset of cells negative for dead cell staining using SYTOX™ Blue Dead Cell Stain, after the removal of doublets. As a negative control, 1000 μM of N-acetyl cysteine was added to the sample 30 min before TBHP.

2.10. RT-qPCR analysis

Total RNA and protein were extracted from cells with NucleoSpin® RNA/Protein (740933.50 [U0933A], Macherey-Nagel, Nordrhein-Westfalen, Germany). Total RNA was purified by ethanol precipitation. 500 μg RNA was reverse transcribed to cDNA by a QuantiTect Reverse Transcription Kit (205313, QIAGEN, Hilden, Germany). Real-time (RT) -qPCR analysis was performed using a TaqMan® Fast Advanced Master Mix (4444556, Thermo Fisher Scientific) by StepOnePlus™ (Thermo Fisher Scientific). Taqman® assays used for analysis are listed in Supplementary Table1. ΔΔCt methods were performed in each analysis using peptidylprolyl isomerase A (*PPIA*) as an internal control gene.

2.11. Western blotting

Protein was measured using BCA assay (23250, Thermo Fisher Scientific). Primary antibodies used for analysis are listed as follows: Glutamate-cysteine ligase (GCL) (ab53179, Abcam, Cambridge, UK), Glutathione reductase (GSR) (LS-C133223, LSBio, Lynwood, WA, USA) and β-Tubulin (Rhodamine conjugated) (#12004166, Biorad). Secondary antibodies used for analysis are listed as follows: StarBright™ Blue 520 Goat Anti-Rabbit IgG (#12005869, Biorad) and StarBright Blue 700 Goat Anti-Mouse IgG (#12004158, Biorad). The membrane was visualized on ChemiDoc (Biorad). The obtained pictures were analyzed with ImageJ (NIH, Bethesda, MD, USA).

2.12. Oxygen measurement

Partial pressure of oxygen (P_aO_2) was measured using an Oxoplate® (OP96F, PreSens, Regensburg, Germany) with HCT116. For 2D culture, cells were seeded at 5.0×10^4 per well and cultured overnight. Spheroids were cultured overnight in a PrimeSurface® 96 slit-well plate at 1.0×10^4 per well. Spheroids were transferred to an Oxoplate at 32 spheroids per well before measurement. CMF 3D was made by mixing 5 mg of CMF with 1.0×10^6 cells and cultured overnight. 200 μL of air-saturated (K_{100}) and 400 μL of oxygen-free water (1 % sodium sulfite, K_0) were prepared and added to each well for calibration. Each method was cultured in phenol red-free DMEM containing 10 % FBS and 1 % antibiotics. Oxygen-free water wells were sealed with opaque film immediately after adding the oxygen-free water to the well. Two wavelengths ($I_{Indicator}$; Ex. 540/Em. 640 and $I_{Reference}$; Ex. 540/Em. 590) were measured by microplate reader (SH-9000/CORONA ELECTRIC Co. Ltd., Ibaraki, Japan). PaO_2 was calculated using the following equation:

$$P_aO_2\ (\text{mmHg}) = 155 \times (K_0 \times I_R^{-1}\text{-}1) \times (K_0 \times K_{100}^{-1}\text{-}1)^{-1}\ I_R = I_{Indicator} \times I_{Reference}^{-1}$$

All samples were run in triplicate.

2.13. Memory function analysis

After culturing for 7 days in each method, cells were collected from each scaffold using the same method described in 2.9 and seeded to a 24-well plate at a density of $5.0 \times 10^4\ cm^{-2}$. Cells were collected on 1, 4, 7 and 11 days after seeding and assayed for intracellular ROS levels using the method described above.

2.14. Histological analysis

After culturing for 7 days in CMF, tissues were fixed in 4 % paraformaldehyde for 3 h, rinsed with PBS several times and embedded into paraffin using CT-Pro20 (Genostaff, Tokyo, Japan). Paraffin blocks were sectioned to 5 μm-thickness, stained with hematoxylin and eosin (HE) and visualized with an optical microscope. For immunological staining, sections were blocked by 1 % bovine serum albumin (BSA) (A3294, Merck, Rahway, NJ, USA)/PBS solution for 20 min at 25 °C and were probed with the primary antibodies diluted in 1 % BSA/PBS solution overnight at 4 °C. Primary antibodies used for analysis are listed as follows: Hypoxia inducing factor 1a (HIF1α) (sc-13515, Santa Cruz Biotechnology, Inc., Dallas, TX, USA), SLC2A1 (sc-377228, Santa Cruz Biotechnology, Inc.), Bcl-2 interacting protein 3 (BNIP3) (#701696, Thermo Fisher Scientific), Pyruvate dehydrogenase kinase 1 (PDK1) (#MA5-15797, Thermo Fisher Scientific). After washing with PBS, the sections were incubated with secondary antibodies diluted in 1 % BSA/PBS solution for 1 h at 25 °C. Secondary antibodies used for analysis are listed as follows; N-Histofine® Simple Stain™ MAX PO(M) (414132F, Nichirei Biosciences Inc., Tokyo, Japan) and N-Histofine® Simple Stain™ MAX PO(R) (414142F, Nichirei Biosciences Inc.). A Liquid DAB + Substrate Chromogen System (K3468, Agilent, Santa Clara, CA, USA) was used for detection and hematoxylin was used for counter staining.

3. Results and discussion

3.1. Characterization of CMF

The white, dried CMF was obtained by homogenizing lyophilized collagen sponge in ethanol. According to the phase contrast photograph (Fig. 2A), the fibers of CMF treated with ethanol were observed to be separated from each other. On the other hand, the fibers of collagen sponge were observed to aggregate in water. In addition, general collagen sponge dissolved easily in the medium, but the dried CMF processed in ethanol did not dissolve once washed in the water. SEM evaluation showed that the collagen sponge was a fiber with a layered, bundled structure and its diameter was around 8 μm, while the fiber diameter of CMF was around 600 nm, and the fibers were disentangled from each other as in the phase contrast microscope images (Fig. 2B and C).

In a previous report, CMF thermally cross-linked in vacuum was also found to be highly dispersible in water. This may be due to dehydration of the surface of collagen molecules at high temperatures, making them hydrophobic, and it is possible that similar dehydration occurs with collagen treated in ethanol. It has been reported that alcohols act on the hydrophobic groups of proteins and stabilize their structure by changing the balance between bulk water and bound water [24], and dehydration with high concentrations of 2-propanol is reported to result in the shrinkage of the D region and the fibril diameter of collagen [25]. Although a higher concentration of hydrous ethanol in the treatment is desirable for the surface dehydration effect, a certain amount of water is necessary to remove the salts in the collagen. Since the amount of triple helix in collagen decreased at ethanol concentrations below 50 %, homogenization and washing were performed in steps of 85 % and 70 % (Figure S1. Supporting Information).

To evaluate the hydrophobicity of the surface of CMF, the fluorescence intensity of sodium 8-Anilino-1-naphthalenesulfonate (ANS-8) was measured. ANS-8 emits only negligible fluorescence at around 540 nm in an aqueous solution, but when ionically bound to hydrophobic sites exposed on the protein surface, the fluorescence intensity increases [26–28]. Fluorescence spectra of the ANS-8 aqueous solution, in which CMF and native collagen were dissolved (Fig. 2D), revealed weak fluorescence detected at around 540 nm under the control condition of PBS

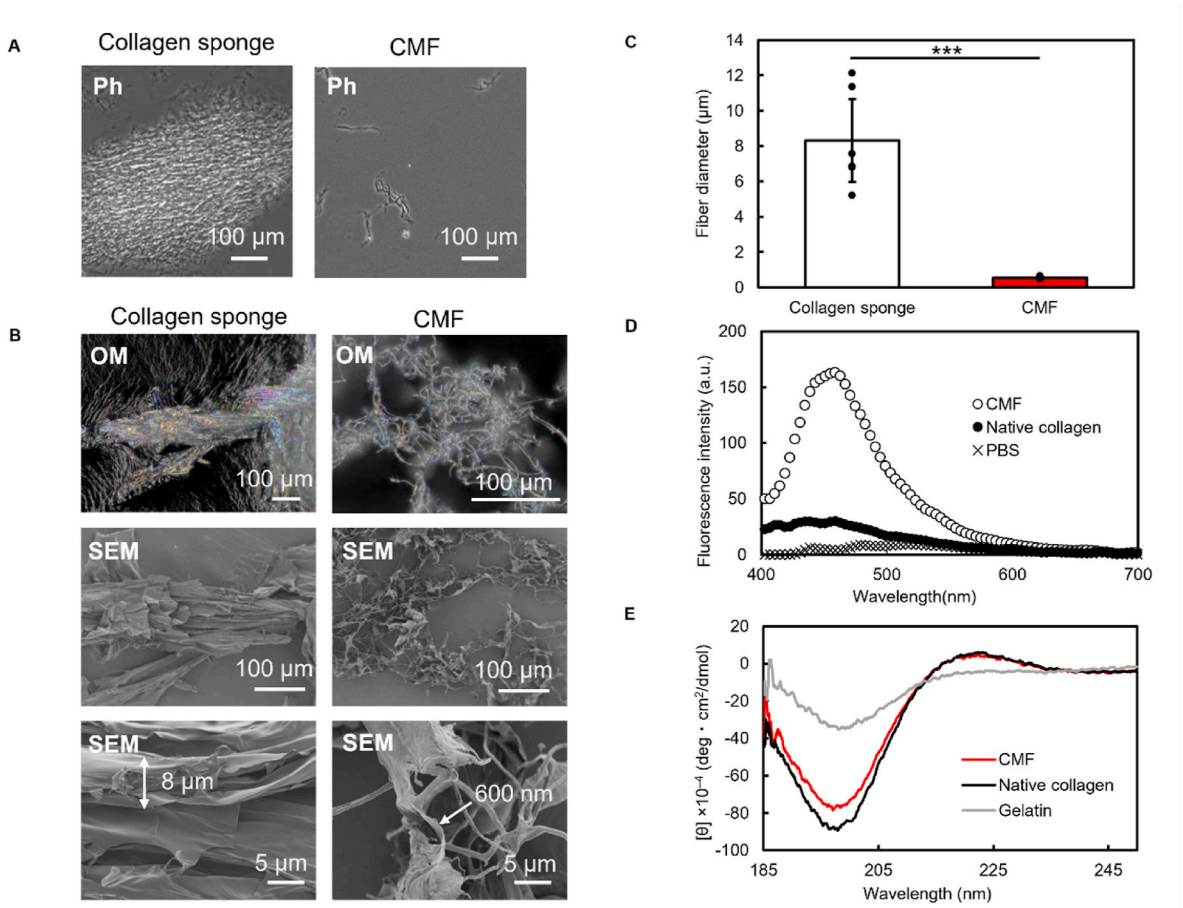

Fig. 2. Structural analyses of CMF. (A) Phase-contrast (Ph) images of collagen sponge fibers and CMF dispersed in water after lyophilization, respectively. (B) Optical microscope (OM) and SEM images of lyophilized collagen sponge and CMF, respectively. (C) Fiber diameter of collagen sponge and CMF calculated from SEM images (n = 6). (D) Fluorescence spectra of 71.4 μM ANS-Mg in CMF and native collagen solution in PBS at 3.5 mg mL^{-1} at 25 °C. Excitation wavelength was 380 nm. (E) CD spectra for CMF, native collagen and gelatin dissolved in 5 μM acetic acid solutions at 5 μg mL^{-1} at 25 °C. Statistical comparison between two groups was analyzed by Student's *t*-test. *p* value, ***<0.001 denotes statistically significant.

+ ANS-8 without protein. With native collagen, a shift of the fluorescence peak to around 450 nm was observed. Furthermore, in CMF, the peak was observed to be more than eight times larger than that in CMF, suggesting that CMF has many hydrophobic domains.

It is commonly reported that proteins, including collagen, may lose their higher-order structure and denature when polar organic solvents are added [29]. With regard to collagen in solution and polar solvents, it has been reported that when collagen is mixed with ethanol at low temperatures, there is no denaturation in the low ethanol concentration range and that the triple helix does not decrease even at around 37 °C up to an ethanol concentration of 40 % [30], but there are few reports evaluating the properties of collagen in a dry state with ethanol. Hence, CD spectral analysis was conducted to evaluate the unique triple helix structure of collagen. The CD spectrum (Fig. 2E) showed that the peak at around 222 nm for CMF was the same as that of the collagen sponge; there was also a peak at the lower wavelength side at around 197 nm, which was slightly reduced in CMF. In general, it has been reported that 222 nm is related to the n-π* transition of amide, and 197 nm is related to the π-π* transition [31]. The positive peak represents the entire triple helix [32], while the negative peak represents structural changes in the peptide chain in collagen [33]. Therefore, the homogenization in ethanol changed the state of some peptides while retaining the higher-order structure of collagen.

3.2. Comparison of ROS resistance in CMF 3D tissue with other culture methods

CMF was considered suitable as a material that could reproduce the high collagen content in the tissue than gel culture due to its hydrophobicity. To construct the 3D model, CMF was mixed with NHDF and HCT116 and precipitated by centrifugation (Fig. 3A), and then CMF 3D tissue was cultured for 7 days. In both cases, HE staining of tissue sections confirmed that the cells were dispersed from the top to the bottom of the 3D tissue (Fig. 3B). Since collagen type I is said to affect the malignancy and stemness of cancer [34], we decided to use this CMF to create and evaluate a 3D cancer model. Although there are reports that collagen plays an important role as a signal source as well as having a physical effect such as on mechanical strength [35], there have been no reports of models that mimic collagen levels comparable to those of living organisms. To evaluate material cytotoxicity, DNA was extracted and quantified from each tissue and the number of viable cells in the tissue was calculated using a calibration curve of cell counts and DNA. The viability of cancer cells in CMF 3D was more than 95 % (Fig. 3C), and no marked difference was observed between CMF 3D and 2D or spheroids.

To assess the characteristics of CMF 3D, tissues were prepared with three different amounts (1, 5 and 10 mg) of CMF, and their elastic modulus was measured. The results indicate that the elastic modulus increases with the amount of CMF (Fig. 4A). Concerning the elasticity of cancer tissue, cancer cells have been reported to exhibit increased

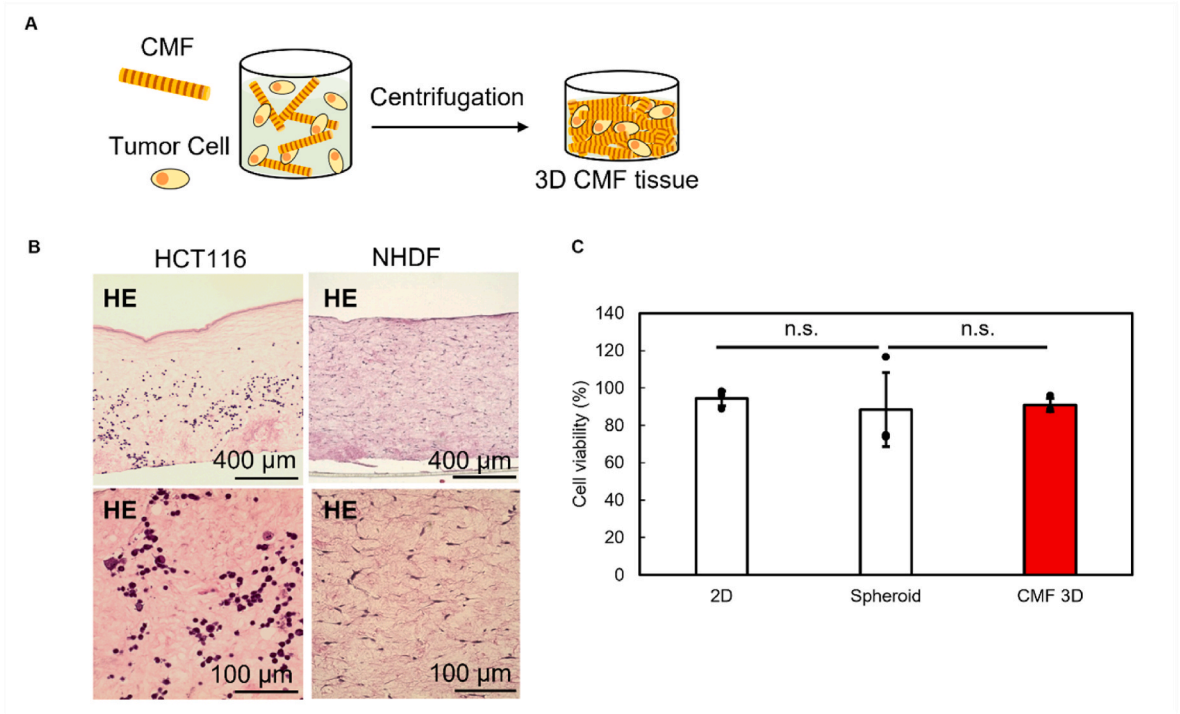

Fig. 3. Developing 3D tissue using CMF. (A) Schematic illustration of the development of CMF 3D tissue. CMF was mixed with a cell suspension and centrifuged at 1150×*g* for 15 min. (B) HE staining images of 3D tissue using 5 mg of CMF mixed with 1.0×10^6 of NHDF and HCT116. (C) Cell viabilities in three culture methods (2D, spheroid, and CMF 3D) based on the cell count after day 1 of culture, relative to the initial seeding cell number. The cell count was calculated from DNA quantity normalized with the calibration curve against the cell number. Statistical comparisons were performed by one-way ANOVA followed by post hoc Tukey-Kramer multiple comparison tests. "n.s." denotes no significant differences.

resistance to cytotoxic drugs in an elasticity-dependent manner in breast cancer and colorectal cancer [36–38]. We evaluated HCT116, a colon cancer cell line, and MDA-MB-231, a breast cancer cell line, as they are known to be affected by the stiffness of their external environment. Based on these reports, we hypothesized that a resistance mechanism, independent of a specific mode of action, may be involved in these phenomena, given the several types of drug resistance reported. Thus, we focused on resistance to ROS, which are involved in cell death and are widely generated stresses in cells. Cancer cells were collected from the scaffold using enzymatic digestion, and ROS were induced by TBHP. After gating living cells using dead cell staining reagent, the number of cells that accumulated ROS was measured using a fluorescent probe for ROS using FACS. The threshold was determined using the fluorescence intensity of the negative control without TBHP and the group of cells below the threshold was defined as ROS-negative cells. According to the histogram of HCT116, cancer cells in CMF 3D exhibited lower ROS accumulation with a fluorescence intensity similar to that of the negative control (Fig. 4B). Then, to calculate the effect of CMF presence on the ROS-negative cells population, CMF 3D tissues were prepared by varying the amount of CMF input to 1, 5, and 10 mg as the conditions for CMF tissue. 2D culture and spheroids were employed as control groups. As mentioned above, the percentage of ROS-negative cells per total cells via gating doublet removal were calculated from the histogram. As qualitatively confirmed on the histogram, the percentage of ROS-resistant cells was highest in CMF tissue, with a marked difference between spheroids and 2D cultures both in HCT116 and MDA-MB-231 (Fig. 4C). This suggested that the cells in the CMF may be scavenging the given ROS. While it has been reported that external stiffness has the highest impact on CD44 expression in HCT116 on 25 kPa scaffold material, and HCT116 cultured on 20 kPa scaffold material exhibits high intracellular accumulation of ROS [39], there are no reported cases regarding resistance to the generated ROS. Moreover, an increase in the ROS-resistant cell population, especially in HCT116, was observed depending on the amount of CMF.

To assess the impact of scaffold stiffness at the gene level, we analyzed the expression of yes-associated protein (*YAP*) and WW Domain Containing Transcription Regulator (*WWTR* or *TAZ*), a drug resistance-related gene in cancer cells linked to scaffold stiffness [40]. However, unlike resistance to ROS, no tendency for gene expression to increase with tissue CMF content was observed (Figure S2. Supporting Information). The stiffness of the CMF tissue may not be the only factor contributing to resistance to ROS, as the CMF tissue can be as stiff as 1–4 kPa.

To investigate the mechanism of this ROS resistance in CMF 3D, we focused on the ROS scavenging process. We focused on GSH, the most abundant endogenous antioxidant, as a ROS scavenger. *GCL* and *GSR*, two enzyme genes directly involved in GSH synthesis, were evaluated. GCL is the rate-limiting enzyme gene in the GSH synthetic pathway. GSR is not an enzyme that directly catalyzes GSH biosynthesis, but it catalyzes the reaction of oxidized glutathione (glutathione disulfide) with NADP + back to its reduced form. Quantitative-PCR analysis showed that the expression of GSH-related genes was 2 to 6-fold higher in HCT116 in CMF 3D than in 2D culture, indicating that ROS resistance in CMF 3D is related to the reduction of ROS by GSH (Fig. 4D). MDA-MB-231 also exhibited a trend toward higher expression in CMF tissue compared to spheroids, though the difference was less pronounced than in HCT116. Considerable expression of this gene was also observed in protein evaluation by Western blotting (Fig. 4E and F) in HCT116.

However, there was no stiffness-dependent increase in CMF expression of glutathione-related genes in any of the tissues, and since the 5 mg condition resulted in the highest expression (Figure S3. Supporting Information), following studies were also limited to 5 mg for evaluation. Additionally, we also evaluated HT29, another colon cancer cell line, to confirm whether the observed trend of ROS resistance and gene expression are common in colon cancers. HT29 showed a similar increase in *GSR*, *GCL*, *YAP*, and *TAZ* expression in the presence of CMF,

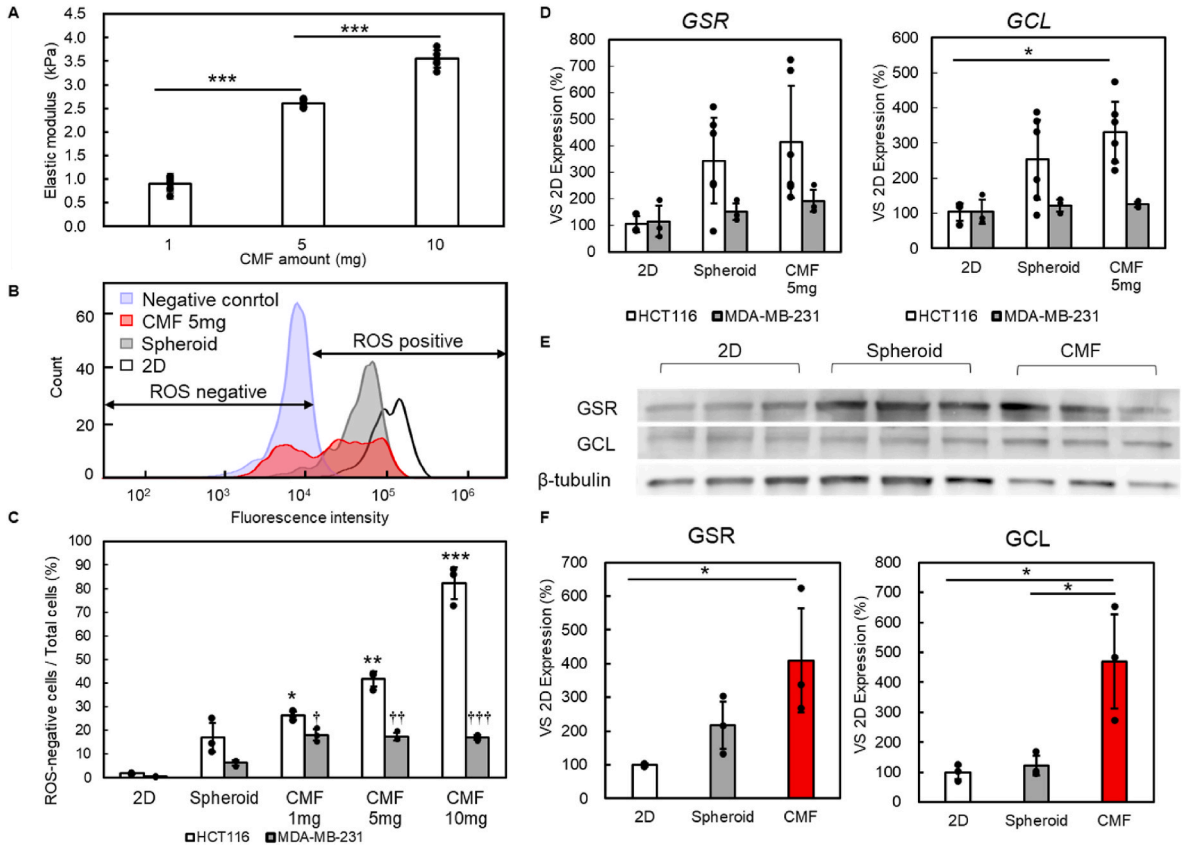

Fig. 4. Evaluation of ROS resistance in CMF 3D. (A) Elastic moduli of CMF tissue constructed under 1, 5, and 10 mg CMF and 1.0×10^6 of HCT116 cells at 25 °C (n = 6). *p* value, ***<0.001 denotes statistically significant. (B) Comparison of histograms of FACS analysis using CellROX™ Deep Red Reagent between 2D, spheroid and CMF 3D culture in HCT116. Cells were cultured using three methods for 7 days and then isolated from the scaffolds. Cells were treated with 100 μM of *tert*-Butyl hydroperoxide (TBHP) and double stained with 1 μM SYTOX™ Blue Nucleic Acid Stain and CellROX™ Deep Red Reagent. Cells below a threshold in the 448/45 channel were defined as live cells and cells below a threshold in the 660/10 channel among live cells were defined as ROS-negative cells. To determine the threshold, 2D cultured cells without TBHP were used as a negative control. (C) The population of ROS-negative cells in total cells via gating of doublet removal of HCT116 and MDA-MB-231 cultured in 2D, spheroid and 1, 5, and 10 mg of CMF 3D for 7 days (n = 3). *** denotes that "CMF 10 mg" is statistically significant at $p < 0.01$ compared to all other samples. ** denotes that "CMF 5 mg" is statistically significant at $p < 0.05$ compared to "CMF 1 mg" and $p < 0.01$ compared to "2D" and "Spheroid". * denotes that "CMF 1 mg" is statistically significant at $p < 0.05$ compared to "2D". ††† denotes that "CMF 10 mg" is statistically significant at $p < 0.01$ compared to "2D" and "Spheroid". †† denotes that "CMF 5 mg" is statistically significant at $p < 0.01$ compared to "2D" and "Spheroid". † denotes that "CMF 1 mg" is statistically significant at $p < 0.01$ compared to "2D" and "Spheroid". (D) Quantitative-PCR analysis of GSH related genes, *GSR* and *GCL* analyzed by the ΔΔCt method from HCT116 and MDA-MB-231 cultured in 2D, spheroid and CMF 3D (5 mg) for 7 days (n ≥ 3). Each target was normalized using *PPIA* as an internal control. Target expressions were compared as a percentage against 2D culture values. *p* value, * <0.05 denote statistically significant. (E) Fluorescence images of WB signals of GSR, GCL and β-tubulin as an internal control from HCT116 cultured in 2D, spheroid and CMF 3D culture for 7 days (n = 3). Full blotting image was displayed in Figure S5. of the Supporting Information. (F) Comparison of GSR and GCL protein expression of HCT116 cultured in 2D, spheroid and CMF 3D (5 mg) for 7 days (n = 3). Each protein expression was calculated from fluorescence intensity from WB images using ImageJ and normalized using β-tubulin as an internal control. Target expressions were compared as a percentage against 2D culture values. *p* value, * <0.05 denote statistically significant. Statistical comparisons were performed by one-way analysis of variance (ANOVA) followed by *post hoc* Tukey-Kramer multiple comparison tests.

despite the lack of confirmed resistance to ROS (Figure S4. Supporting Information). No stiffness-dependent increasing trend of CMF was observed in each gene of HT29 because CMF 1 mg exhibiting the highest expression level. The optimal amount of CMF may be freely adjustable, although it varies depending on the state of the cancer cells.

3.3. Comparison of partial oxygen pressure and hypoxic marker expression in CMF3D tissue with other culture methods

The differences in ROS resistance and GSH-related enzymes between CMF 3D and other culture methods identified in this study can be attributed to their different tissue sizes. The spheroids created in this study were approximately 100 μm in diameter, whereas the CMF 3D tissue was approximately 3 mm thick (Figure S6, Supporting Information). It was suggested that this CMF 3D thickness may create hypoxic conditions. Therefore, we attempted to measure oxygen partial pressure (Fig. 5A). The general "normal oxygen" environment is said to be around 150 mmHg [41]. On the other hand, spheroids, which are said to mimic hypoxic conditions as a conventional culture method, showed a lower oxygen concentration than 2D at 16 mmHg. However, since the hypoxic environment, commonly referred to as "hypoxia", is 8–10 mmHg, spheroids are not able to replicate the *in vivo* tumor environment. On the other hand, the partial pressure of oxygen in CMF 3D is about 10 mmHg [42], suggesting that only CMF mimics the oxygen concentration of tumors *in vivo* in the same 3D culture.

To assess whether this oxygen state is actually linked to the expression of hypoxia-related genes in the cell, quantitative-PCR analysis was performed on the commonly used hypoxia marker gene *HIF1α* and other hypoxia marker genes derived from *HIF1α* (*SLC2A1*, *PDK1*, *BNIP3*). *HIF1α* is a gene that synthesizes a transcription factor that is activated when cells are hypoxic and is widely used as a general hypoxia marker. However, gene expression analysis in this study showed slight difference in *HIF1α* expression among the three culture methods. Rather, expression was lower in CMF 3D than in the other two, even though CMF 3D

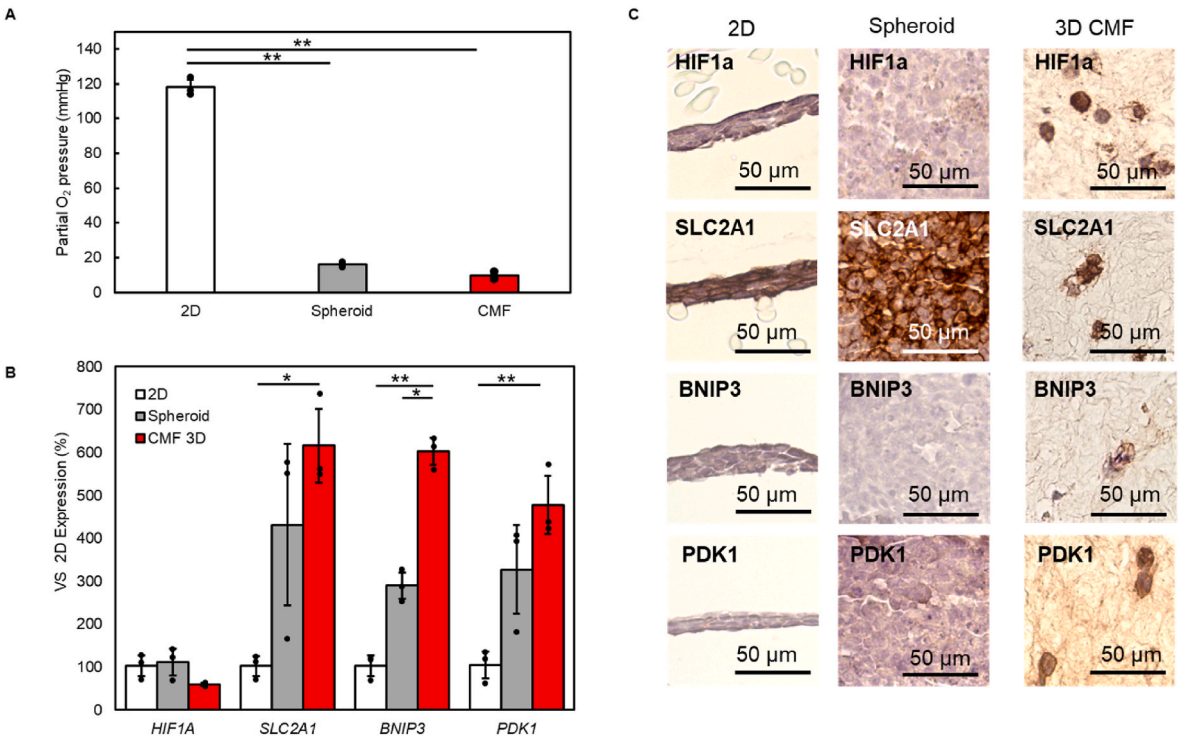

Fig. 5. Evaluation of hypoxic condition in CMF 3D. (A) Comparison of Partial O_2 pressure in tissue using an Oxoplate® (n = 3). HCT116 were seeded on each well of an Oxoplate in 2D, spheroid and CMF 3D. The bottom fluorescence intensity of the plate was measured. Fluorescence intensity at Ex. 540 nm/Em 650 nm was used as an indicator, while Ex. 540 nm/Em 590 nm was used as a reference. Both were used for calculation of O_2 saturation (%) after calibration using O_2 saturated water and O_2 free water at 25 °C. Oxygen partial pressure (mmHg) was calculated from oxygen saturation at 20 °C and atmospheric pressure of 1013 hPa. (B) Quantitative-PCR analysis of hypoxia related genes, *HIF1α*, *SLC2A1*, *BNIP3* and *PDK1* analyzed by the ΔΔCt method from HCT116 cultured in 2D, spheroid and CMF 3D (5 mg) for 7 days (n = 3). Each target was normalized using *PPIA* as an internal control. Target expressions were compared as a percentage against 2D culture values. (C) Immunohistochemical images of paraffin cross sections of 2D, spheroid and CMF 3D tissues. Statistical comparisons were performed by one-way ANOVA followed by *post hoc* Tukey-Kramer multiple comparison tests. *p* value, * <0.05 and ** <0.01 denote statistically significant.

has the lowest partial pressure of oxygen in the tissue (Fig. 5B).

In contrast, expression of the other three genes was increased in 2D < spheroids < CMF, suggesting that CMF cells are still affected by other hypoxia marker systems. As for *HIF1α*, there were differences between gene expression and immunostaining results (Fig. 5C), but it has been reported that *HIF1α* often produces results that do not correlate with gene expression and protein expression [43]. One possible reason for this is that *HIF1α* is a marker expressed in response to acute hypoxia. It has been reported that in prostate cancer, *HIF1α* expression is maximal within 4 h of being placed in hypoxic conditions, and then decreases with continued incubation under hypoxic conditions [44]. Since the culture conditions in this study were 7 days, the *HIF1α* gene was probably already degraded at the time of assay. In relation to glutathione synthesis, *SLC2A1* and *PDK1* are involved in the supply of NADPH required for GSH reduction through glycolysis activation [45].

3.4. *"Cell memory function" in CMF 3D tissue*

In the previous section, it was revealed that cancer cells cultured in CMFs tend to acquire ROS resistance and become malignant through hypoxia-mediated modulation of the GSH synthesis pathway. It is well known that any cancer cells that remain in the body after surgical removal can become malignant and survive *in vivo*, causing recurrence and metastasis. In other words, malignant cancer cells are thought to maintain their acquired characteristics for a long period of time despite changes in the surrounding environment though few reports have evaluated whether *in vitro* models can maintain the acquired malignancy of cancer cells. HCT116 cultured by each of the three methods were isolated from the scaffold and seeded in 2D. Cells were collected 0, 1, 4, 7, and 11 days after 2D seeding and evaluated for ROS resistance (Fig. 6A). The results showed that cells isolated from CMF 3D (Ex CMF) remained highly ROS resistant from immediately after isolation from the scaffold until day 11 (Fig. 6B). Conversely, cells isolated from 2D (Ex 2D) and spheroids (Ex spheroid) had low ROS resistance at the beginning of isolation, and the number of resistant cells gradually increased as the number of days of culture increased. Finally, all culture methods resulted in a higher percentage of ROS resistant cells on day 11. The gradual increase in ROS resistance observed in Ex 2D and Ex spheroids after isolation may be due to increased intercellular adhesion due to increased cell density, rather than to the retention of properties acquired by cells during culture, as in Ex CMF. This is probably due to the propensity of cancer cells to continue to proliferate after becoming confluent; it is unlikely that such a phenomenon would occur in normal cells.

To corroborate these results, the changes in *GSR* and *GCL* gene expression over time were also evaluated. It was found that *GSR* expression at the time of collection (Day 0) was higher in Ex CMF than in the other two culture methods, but then gradually decreased in a manner similar to the trend observed for ROS resistance (Fig. 6C). In *GCL*, the same trend of higher Ex CMF on Day 0 was observed, but the cells behaved differently from ROS resistance and *GSR* expression, with Ex CMF and Ex spheroids having the highest expression on Day 1. This difference may involve the regulatory pathways of *GSR* and *GCL*. Unlike *GSR*, *GCL* is known to be directly regulated by GSH levels. Upon collection from Day 0 tissue, both spheroids and CMF 3D recover from their 3D dense cell-to-cell state and return to two dimensions, resulting in a change in the flux of medium volume per cell [46]. Thus, it is possible that the *GCL* is upregulated after 1 day in response to feedback from the temporary decrease in pericellular GSH content. To confirm this, it is necessary to quantify the amount of GSH at the time of

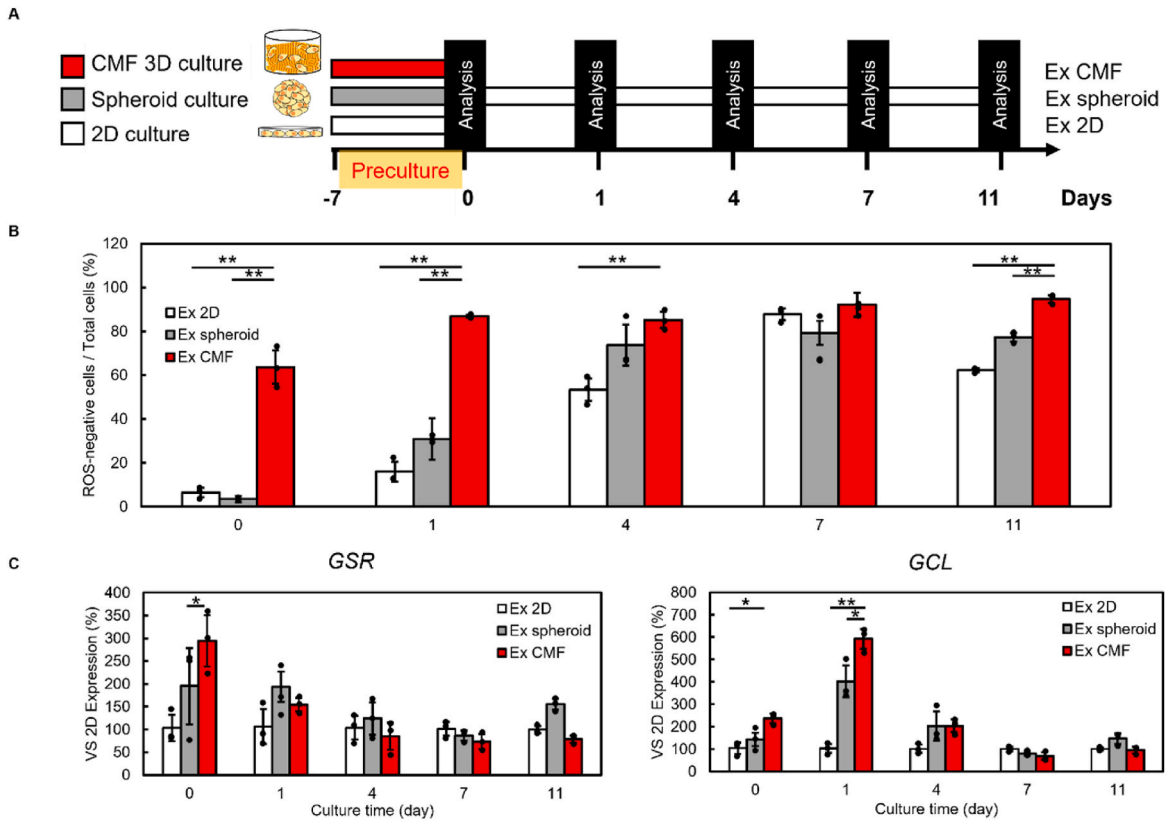

Fig. 6. Evaluation of "memory function" of cells in CMF 3D. (A) Schematic illustration of culture scheme to evaluate "memory function" of cells. HCT116 were precultured in each culture method (2D, spheroid, CMF 3D) and isolated using enzymes from their scaffold. All isolated cells (Ex 2D, Ex spheroid and Ex CMF) were seeded to 2D culture for 11 days and ROS resistance was evaluated at Day 0, 1, 4, 7 and 11. (B) The change in the percentage of ROS-negative cells in total cells via gating of doublet removal from Day 0 to Day 11 was analyzed in Ex 2D, Ex spheroid, and Ex CMF. (C) Quantitative-PCR analysis of GSH related genes, *GSR* and *GCL* analyzed by the ΔΔCt method from HCT116 cultured in Ex 2D, Ex spheroid and Ex CMF (n = 3) from Day 0 to Day 11. Each target was normalized using *PPIA* as an internal control. Target expressions were compared as a percentage against 2D culture values. Statistical comparisons were performed by one-way ANOVA followed by *post hoc* Tukey-Kramer multiple comparison tests. *p* value, * <0.05 and ** <0.01 denote statistically significant.

collection and in subsequent cultures.

What contributes to this long-term change in cellular properties requires further analysis, but there are several possible factors. First, hypoxia is known to activate various pathways in cancer cells and has been reported to increase invasive potential and to transform cancer cells into a more undifferentiated state [47,48]. To assess this hypothesis, gene expression analysis using *CD44* and *CD44v9*, commonly used as stem cell markers for colon cancer cells, revealed a gradual decrease in expression in both Ex spheroid and Ex CMF. Although there was no difference between the Ex spheroid and Ex CMF tissues, both confirm that the 3D culture history affected the properties of the cells (Figure S7. Supporting Information). Another hypothesis is that the stiffness of the scaffold material plays a role. This is because *YAP* induced by the hardness of the external environment has been reported to interact with histone methyltransferase *MII1*, an epigenetics-related gene, in colorectal cancer, possibly causing persistent genetic mutations, which may be related to cancer cell plasticity [49]. It is possible that CMF-induced changes in the stiffness of the scaffold may affect long-term changes in the properties of the cells via YAP activation.

It is also known that ECM receptors on the cell surface can alter the properties of cancer cells [50]. In particular, the binding of excess amounts of collagen to integrin β-subunits is known to activate src family kinases, leading to the formation of focal adhesion, which in turn promote cancer cell proliferation. In addition, the downstream signaling cascade, such as MEK (Mitogen-activated protein kinase) and ERK (Extracellular signal-Regulated Kinase), are known to activate the aforementioned hypoxia-related genes, which may also contribute to the acquisition of ROS resistance via hypoxia-induced signaling [51,52]. From these considerations, it is likely that the unique properties of CMF, which combine high collagen density, hypoxia, and moderate stiffness, combine to affect the memory function of cancer cells. To investigate this mechanism in more detail, the effects of the presence or absence of CMF would need to be investigated using comprehensive genetic analysis to examine the expression associations of ECM receptors, hypoxia-related genes, and their downstream signaling pathways.

4. Conclusion

Homogenization in ethanol was used to create CMF that were highly dispersible in a dry state. Cancer cell line embedded in CMF were prepared by centrifugal sedimentation as CMF 3D tissue, and the cells in CMF tended to have higher ROS resistance to cancer cells compared to spheroid and 2D culture. This may be due to an increase in GSH synthesis-related genes, suggesting that hypoxia in the CMF tissue is involved. The ROS resistance of the cells in the CMF was maintained for about a week after the cells were separated from the scaffold and returned to 2D culture.

CRediT authorship contribution statement

Asuka Yamada: Writing – review & editing, Writing – original draft, Visualization, Investigation. **Shiro Kitano:** Supervision, Conceptualization. **Michiya Matsusaki:** Writing – review & editing, Supervision, Methodology, Conceptualization.

Declaration of competing interest

The authors declare the following financial interests/personal relationships which may be considered as potential competing interests:

Michiya Matsusaki reports financial support was provided by JST-Mirai Program. Michiya MATSUSAKI reports a relationship with JST-Mirai Program that includes: funding grants. Michiya MATSUSAKI reports a relationship with COI-NEXT that includes: funding grants. Michiya MATSUSAKI reports a relationship with New Energy and Industrial Technology Development Organization that includes: funding grants. Michiya MATSUSAKI reports a relationship with Grant-in-Aid for Scientific Research (A) that includes: funding grants. Michiya MATSUSAKI has patent #PCT/JP2022/026062 issued to Assignee. If there are other authors, they declare that they have no known competing financial interests or personal relationships that could have appeared to influence the work reported in this paper.

Data availability

Data will be made available on request.

Acknowledgment

The authors acknowledge financial supports by Mirai-Program (18077228) and COI-NEXT (JPMJPF2009) from JST, JPNP20004 from NEDO, Grant-in-Aid for Scientific Research (A) (20H00665).

Appendix A. Supplementary data

Supplementary data to this article can be found online at https://doi.org/10.1016/j.mtbio.2024.101097.

References

[1] C. Yang, M.W. Tibbitt, L. Basta, K.S. Anseth, Mechanical memory and dosing influence stem cell fate, Nat. Mater. 13 (2014) 645–652, https://doi.org/10.1038/nmat3889.

[2] J.S. Silver, K.A. Günay, A.A. Cutler, T.O. Vogler, T.E. Brown, B.T. Pawlikowski, O. J. Bednarski, K.L. Bannister, C.J. Rogowski, A.G. Mckay, F.W. DelRio, B.B. Olwin, K.S. Anseth, Injury-mediated stiffening persistently activates muscle stem cells through YAP and TAZ mechanotransduction, Sci. Adv. 7 (2021) eabe4501, https://doi.org/10.1126/sciadv.abe4501.

[3] C.J. Walker, C. Crocini, D. Ramirez, A.R. Killaars, J.C. Grim, B.A. Aguado, K. Clark, M.A. Allen, R.D. Dowell, L.A. Leinwand, K.S. Anseth, Nuclear mechanosensing drives chromatin remodelling in persistently activated fibroblasts, Nat. Biomed. Eng. 5 (2021) 1485–1499, https://doi.org/10.1038/s41551-021-00709-w.

[4] S. Kawano, M. Kojima, Y. Higuchi, M. Sugimoto, K. Ikeda, N. Sakuyama, S. Takahashi, R. Hayashi, A. Ochiai, N. Saito, Assessment of elasticity of colorectal cancer tissue, clinical utility, pathological and phenotypical relevance, Cancer Sci. 106 (2015) 1232–1239, https://doi.org/10.1111/cas.12720.

[5] Y. Shen, X. Wang, J. Lu, M. Salfenmoser, N.M. Wirsik, N. Schleussner, A. Imle, A. Freire Valls, P. Radhakrishnan, J. Liang, G. Wang, T. Muley, M. Schneider, C. Ruiz De Almodovar, A. Diz-Muñoz, T. Schmidt, Reduction of liver metastasis stiffness improves response to bevacizumab in metastatic colorectal cancer, Cancer Cell 37 (2020) 800–817.e7, https://doi.org/10.1016/j.ccell.2020.05.005.

[6] L.T.H. Phi, I.N. Sari, Y.-G. Yang, S.-H. Lee, N. Jun, K.S. Kim, Y.K. Lee, H.Y. Kwon, Cancer stem cells (CSCs) in drug resistance and their therapeutic implications in cancer treatment, Stem Cell. Int. 2018 (2018) 5416923, https://doi.org/10.1155/2018/5416923.

[7] K.B. Myant, P. Cammareri, E.J. McGhee, R.A. Ridgway, D.J. Huels, J.B. Cordero, S. Schwitalla, G. Kalna, E.-L. Ogg, D. Athineos, P. Timpson, M. Vidal, G.I. Murray, F.R. Greten, K.I. Anderson, O.J. Sansom, ROS production and NF-κB activation triggered by RAC1 facilitate WNT-driven intestinal stem cell proliferation and colorectal cancer initiation, Cell Stem Cell 12 (2013) 761–773, https://doi.org/10.1016/j.stem.2013.04.006.

[8] T. Gura, Systems for identifying new drugs are often faulty, Science 278 (1997) 1041–1042, https://doi.org/10.1126/science.278.5340.1041.

[9] C. Jensen, Y. Teng, Is it time to start transitioning from 2D to 3D cell culture? Front. Mol. Biosci. 7 (2020) https://doi.org/10.3389/fmolb.2020.00033.

[10] G.L. Semenza, Intratumoral hypoxia and mechanisms of immune evasion mediated by hypoxia-inducible factors, Physiology 36 (2021) 73–83, https://doi.org/10.1152/physiol.00034.2020.

[11] G. Lazzari, V. Nicolas, M. Matsusaki, M. Akashi, P. Couvreur, S. Mura, Multicellular spheroid based on a triple co-culture: a novel 3D model to mimic pancreatic tumor complexity, Acta Biomater. 78 (2018) 296–307, https://doi.org/10.1016/j.actbio.2018.08.008.

[12] F. Hirschhaeuser, H. Menne, C. Dittfeld, J. West, W. Mueller-Klieser, L.A. Kunz-Schughart, Multicellular tumor spheroids: an underestimated tool is catching up again, J. Biotechnol. 148 (2010) 3–15, https://doi.org/10.1016/j.jbiotec.2010.01.012.

[13] Y. Tan, D. Chen, Y. Wang, W. Wang, L. Xu, R. Liu, C. You, G. Li, H. Zhou, D. Li, Limbal bio-engineered tissue employing 3D nanofiber-aerogel scaffold to facilitate LSCs growth and migration, Macromol. Biosci. 22 (2022) 2100441, https://doi.org/10.1002/mabi.202100441.

[14] D. Fan, U. Staufer, A. Accardo, Engineered 3D polymer and hydrogel microenvironments for cell culture applications, Bioengineering 6 (2019) 113, https://doi.org/10.3390/bioengineering6040113.

[15] A. Nishiguchi, M. Matsusaki, M.R. Kano, H. Nishihara, D. Okano, Y. Asano, H. Shimoda, S. Kishimoto, S. Iwai, M. Akashi, In vitro 3D blood/lymph-vascularized human stromal tissues for preclinical assays of cancer metastasis, Biomaterials 179 (2018) 144–155, https://doi.org/10.1016/j.biomaterials.2018.06.019.

[16] Y. Naito, Y. Yoshinouchi, Y. Sorayama, H. Kohara, S. Kitano, S. Irie, M. Matsusaki, Constructing vascularized hepatic tissue by cell-assembled viscous tissue sedimentation method and its application for vascular toxicity assessment, Acta Biomater. 140 (2022) 275–288, https://doi.org/10.1016/j.actbio.2021.11.027.

[17] G. Lai, Y. Li, G. Li, Effect of concentration and temperature on the rheological behavior of collagen solution, Int. J. Biol. Macromol. 42 (2008) 285–291, https://doi.org/10.1016/j.ijbiomac.2007.12.010.

[18] K. Tarnutzer, D. Siva Sankar, J. Dengjel, C.Y. Ewald, Collagen constitutes about 12% in females and 17% in males of the total protein in mice, Sci. Rep. 13 (2023) 4490, https://doi.org/10.1038/s41598-023-31566-z.

[19] Y. Naka, S. Kitano, S. Irie, M. Matsusaki, Wholly vascularized millimeter-sized engineered tissues by cell-sized microscaffolds, Mater Today Bio 6 (2020) 100054, https://doi.org/10.1016/j.mtbio.2020.100054.

[20] H. Liu, S. Kitano, S. Irie, R. Levato, M. Matsusaki, Collagen microfibers induce blood capillary orientation and open vascular lumen, Advanced Biosystems 4 (2020) 2000038, https://doi.org/10.1002/adbi.202000038.

[21] N. Sasaki, H. Takeuchi, S. Kitano, S. Irie, A. Amano, M. Matsusaki, Dynamic analysis of Porphyromonas gingivalis invasion into blood capillaries during the infection process in host tissues using a vascularized three-dimensional human gingival model, Biomater. Sci. 9 (2021) 6574–6583, https://doi.org/10.1039/D1BM00831E.

[22] F. Louis, S. Kitano, J.F. Mano, M. Matsusaki, 3D collagen microfibers stimulate the functionality of preadipocytes and maintain the phenotype of mature adipocytes for long term cultures, Acta Biomater. 84 (2019) 194–207, https://doi.org/10.1016/j.actbio.2018.11.048.

[23] D.-H. Kang, F. Louis, H. Liu, H. Shimoda, Y. Nishiyama, H. Nozawa, M. Kakitani, D. Takagi, D. Kasa, E. Nagamori, S. Irie, S. Kitano, M. Matsusaki, Engineered whole cut meat-like tissue by the assembly of cell fibers using tendon-gel integrated bioprinting, Nat. Commun. 12 (2021) 5059, https://doi.org/10.1038/s41467-021-25236-9.

[24] R. Usha, R. Maheshwari, A. Dhathathreyan, T. Ramasami, Structural influence of mono and polyhydric alcohols on the stabilization of collagen, Colloids Surf. B Biointerfaces 48 (2006) 101–105, https://doi.org/10.1016/j.colsurfb.2006.01.015.

[25] H.C. Wells, K.H. Sizeland, S.J.R. Kelly, N. Kirby, A. Hawley, S. Mudie, R. G. Haverkamp, Collagen fibril intermolecular spacing changes with 2-propanol: a mechanism for tissue stiffness, ACS Biomater. Sci. Eng. 3 (2017) 2524–2532, https://doi.org/10.1021/acsbiomaterials.7b00418.

[26] I. Sirangelo, E. Bismuto, S. Tavassi, G. Irace, Apomyoglobin folding intermediates characterized by the hydrophobic fluorescent probe 8-anilino-1-naphthalene sulfonate (ANS), Biochim. Biophys. Acta Protein Struct. Mol. Enzymol. 1385 (1998) 69–77, https://doi.org/10.1016/S0167-4838(98)00038-7.

[27] J. Slavík, Anilinonaphthalene sulfonate as a probe of membrane composition and function, Biochim. Biophys. Acta 694 (1982) 1–25, https://doi.org/10.1016/0304-4157(82)90012-0.

[28] M. Deshpande, S.K. Sathe, Interactions with 8-Anilinonaphthalene-1-sulfonic acid (ANS) and surface hydrophobicity of black gram (vigna mungo) phaseolin, J. Food Sci. 83 (2018) 1847–1855, https://doi.org/10.1111/1750-3841.14204.

[29] G. Shanmugam, S.M.M. Reddy, B. Madhan, J.R. Rao, Method of addition of acetonitrile influences the structure and stability of collagen, Process Biochem. 49 (2014) 210–216, https://doi.org/10.1016/j.procbio.2013.11.013.

[30] A. Gopinath, S.M.M. Reddy, B. Madhan, G. Shanmguam, J.R. Rao, Effect of aqueous ethanol on the triple helical structure of collagen, Eur. Biophys. J. 43 (2014) 643–652, https://doi.org/10.1007/s00249-014-0994-5.

[31] K. Matsuo, R. Yonehara, K. Gekko, Secondary-structure analysis of proteins by vacuum-ultraviolet circular dichroism spectroscopy, J. Biochem. 135 (2004) 405–411, https://doi.org/10.1093/jb/mvh048.

[32] K.E. Drzewiecki, D.R. Grisham, A.S. Parmar, V. Nanda, D.I. Shreiber, Circular dichroism spectroscopy of collagen fibrillogenesis: a new use for an old technique, Biophys. J. 111 (2016) 2377–2386, https://doi.org/10.1016/j.bpj.2016.10.023.

[33] J.L.S. Lopes, A.J. Miles, L. Whitmore, B.A. Wallace, Distinct circular dichroism spectroscopic signatures of polyproline II and unordered secondary structures: applications in secondary structure analyses, Protein Sci. 23 (2014) 1765–1772, https://doi.org/10.1002/pro.2558.

[34] S.C. Kirkland, Type I collagen inhibits differentiation and promotes a stem cell-like phenotype in human colorectal carcinoma cells, Br. J. Cancer 101 (2009) 320–326, https://doi.org/10.1038/sj.bjc.6605143.

[35] Y. Shintani, Y. Fukumoto, N. Chaika, R. Svoboda, M.J. Wheelock, K.R. Johnson, Collagen I–mediated up-regulation of N-cadherin requires cooperative signals from

integrins and discoidin domain receptor 1, J. Cell Biol. 180 (2008) 1277–1289, https://doi.org/10.1083/jcb.200708137.
[36] S. Zustiak, R. Nossal, D.L. Sackett, Multiwell stiffness assay for the study of cell responsiveness to cytotoxic drugs, Biotechnol. Bioeng. 111 (2014) 396–403, https://doi.org/10.1002/bit.25097.
[37] L. Hui, J. Zhang, X. Ding, X. Guo, X. Jiang, Matrix stiffness regulates the proliferation, stemness and chemoresistance of laryngeal squamous cancer cells, Int. J. Oncol. 50 (2017) 1439–1447, https://doi.org/10.3892/ijo.2017.3877.
[38] M.H. Joyce, C. Lu, E.R. James, R. Hegab, S.C. Allen, L.J. Suggs, A. Brock, Phenotypic basis for matrix stiffness-dependent chemoresistance of breast cancer cells to doxorubicin, Front. Oncol. 8 (2018). doi: 10.3389/fonc.2018.00337.
[39] E. Jabbari, S.K. Sarvestani, L. Daneshian, S. Moeinzadeh, Optimum 3D matrix stiffness for maintenance of cancer stem cells is dependent on tissue origin of cancer cells, PLoS One 10 (2015) e0132377, https://doi.org/10.1371/journal.pone.0132377.
[40] Y. Zhou, Y. Wang, W. Zhou, T. Chen, Q. Wu, V.K. Chutturghoon, B. Lin, L. Geng, Z. Yang, L. Zhou, S. Zheng, YAP promotes multi-drug resistance and inhibits autophagy-related cell death in hepatocellular carcinoma via the RAC1-ROS-mTOR pathway, Cancer Cell Int. 19 (2019) 179, https://doi.org/10.1186/s12935-019-0898-7.
[41] I.V. Kelmanson, A.G. Shokhina, D.A. Kotova, M.S. Pochechuev, A.D. Ivanova, A. I. Kostyuk, A.S. Panova, A.A. Borodinova, M.A. Solotenkov, E.A. Stepanov, R. I. Raevskii, A.A. Moshchenko, V.V. Pak, Y.G. Ermakova, G.J.C. van Belle, V. Tarabykin, P.M. Balaban, I.V. Fedotov, A.B. Fedotov, M. Conrad, I. Bogeski, D. M. Katschinski, T.R. Doeppner, M. Bähr, A.M. Zheltikov, V.V. Belousov, D.S. Bilan, In vivo dynamics of acidosis and oxidative stress in the acute phase of an ischemic stroke in a rodent model, Redox Biol. 48 (2021) 102178, https://doi.org/10.1016/j.redox.2021.102178.
[42] M. Hockel, P. Vaupel, Tumor hypoxia: definitions and current clinical, biologic, and molecular aspects, JNCI Journal of the National Cancer Institute 93 (2001) 266–276, https://doi.org/10.1093/jnci/93.4.266.
[43] L.W.S. Finley, A. Carracedo, J. Lee, A. Souza, A. Egia, J. Zhang, J. Teruya-Feldstein, P.I. Moreira, S.M. Cardoso, C.B. Clish, P.P. Pandolfi, M.C. Haigis, SIRT3 opposes reprogramming of cancer cell metabolism through HIF1α destabilization, Cancer Cell 19 (2011) 416–428, https://doi.org/10.1016/j.ccr.2011.02.014.
[44] L. Ravenna, L. Principessa, A. Verdina, L. Salvatori, M.A. Russo, E. Petrangeli, Distinct phenotypes of human prostate cancer cells associate with different adaptation to hypoxia and pro-inflammatory gene expression, PLoS One 9 (2014) e96250, https://doi.org/10.1371/journal.pone.0096250.
[45] P. Jiang, W. Du, M. Wu, Regulation of the pentose phosphate pathway in cancer, Protein & Cell 5 (2014) 592–602, https://doi.org/10.1007/s13238-014-0082-8.
[46] W. Langston, W. Li, L. Harrison, T.Y. Aw, Activation of promoter activity of the catalytic subunit of γ-glutamylcysteine ligase (GCL) in brain endothelial cells by insulin requires antioxidant response element 4 and altered glycemic status: implication for GCL expression and GSH synthesis, Free Radic. Biol. Med. 51 (2011) 1749–1757, https://doi.org/10.1016/j.freeradbiomed.2011.08.004.
[47] B. Das, R. Tsuchida, D. Malkin, G. Koren, S. Baruchel, H. Yeger, Hypoxia enhances tumor stemness by increasing the invasive and tumorigenic side population fraction, Stem Cell. 26 (2008) 1818–1830, https://doi.org/10.1634/stemcells.2007-0724.
[48] A. Jögi, I. Øra, H. Nilsson, Å. Lindeheim, Y. Makino, L. Poellinger, H. Axelson, S. Påhlman, Hypoxia alters gene expression in human neuroblastoma cells toward an immature and neural crest-like phenotype, Proc. Natl. Acad. Sci. USA 99 (2002) 7021–7026, https://doi.org/10.1073/pnas.102660199.
[49] J. Heuberger, J. Grinat, F. Kosel, L. Liu, S. Kunz, R.O. Vidal, M. Keil, J. Haybaeck, S. Robine, D. Louvard, C. Regenbrecht, A. Sporbert, S. Sauer, B. von Eyss, M. Sigal, W. Birchmeier, High Yap and Mll1 promote a persistent regenerative cell state induced by Notch signaling and loss of p53, Proc. Natl. Acad. Sci. USA 118 (2021) e2019699118, https://doi.org/10.1073/pnas.2019699118.
[50] H. Huang, S. Wright, J. Zhang, R.A. Brekken, Getting a grip on adhesion: cadherin switching and collagen signaling, Biochim. Biophys. Acta Mol. Cell Res. 1866 (2019) 118472, https://doi.org/10.1016/j.bbamcr.2019.04.002.
[51] A.R. Poh, M. Ernst, Functional roles of SRC signaling in pancreatic cancer: recent insights provide novel therapeutic opportunities, Oncogene 42 (2023) 1786–1801, https://doi.org/10.1038/s41388-023-02701-x.
[52] M.J. Lamberti, M.F. Pansa, R.E. Vera, M.E. Fernández-Zapico, N.B. Rumie Vittar, V. A. Rivarola, Transcriptional activation of HIF-1 by a ROS-ERK axis underlies the resistance to photodynamic therapy, PLoS One 12 (2017) e0177801, https://doi.org/10.1371/journal.pone.0177801.